



Decadal increases in carbon uptake offset by respiratory losses across northern permafrost ecosystems

Received: 26 July 2023

A list of authors and their affiliations appears at the end of the paper

Accepted: 5 June 2024

Published online: 26 July 2024

Check for updates

Tundra and boreal ecosystems encompass the northern circumpolar permafrost region and are experiencing rapid environmental change with important implications for the global carbon (C) budget. We analysed multi-decadal time series containing 302 annual estimates of carbon dioxide (CO_2) flux across 70 permafrost and non-permafrost ecosystems, and 672 estimates of summer CO_2 flux across 181 ecosystems. We find an increase in the annual CO_2 sink across non-permafrost ecosystems but not permafrost ecosystems, despite similar increases in summer uptake. Thus, recent non-growing-season CO_2 losses have substantially impacted the CO_2 balance of permafrost ecosystems. Furthermore, analysis of interannual variability reveals warmer summers amplify the C cycle (increase productivity and respiration) at putatively nitrogen-limited sites and at sites less reliant on summer precipitation for water use. Our findings suggest that water and nutrient availability will be important predictors of the C-cycle response of these ecosystems to future warming.

High-latitude ecosystems store nearly half the terrestrial C stocks¹. The northern circumpolar permafrost region, which includes most of the tundra biome and a large fraction of the boreal forest biome², represents only 15% of the Earth's soil area but stores approximately one-third (approximately 1,460–1,600 Pg) of global soil organic C^{3–5}. Permafrost ecosystems are currently warming three to four times faster than the global mean^{6,7}, making this critical soil C pool increasingly vulnerable to decomposition. Although increased plant C uptake may offset some portion of soil C losses, the climate impact of CO_2 and methane (CH_4) C emissions from the permafrost region over the next century will likely be comparable to a high-emissions nation³. However, these permafrost losses are not accounted for in the emissions targets set forth in the Paris accord⁸. Evidence from remote sensing and modelling efforts suggest that both gross primary productivity (GPP)^{9–13} and ecosystem respiration (R_{eco})^{9–12} are increasing across high latitudes; however, the magnitude of this C-cycle amplification and its effect on decadal trends in the net ecosystem exchange (NEE; the relatively small difference between GPP and R_{eco}) of CO_2 with the atmosphere remain highly uncertain^{3,5,14–16}.

Previous ground-based syntheses of decadal changes in NEE in permafrost ecosystems were limited by a scarcity of year-round (annual) measurements, leading to contradictory conclusions^{9,17}. Between 1990 and 2009, annual NEE measurements binned by decade suggested that tundra ecosystems were becoming an increasing CO_2 sink (accumulating ecosystem C over time)¹⁷. However, a separate analysis of the same time period based on the difference between trends of growing-season and non-growing-season NEE suggested that upland tundra ecosystems were becoming an increasing CO_2 source (losing ecosystem C over time)⁹. Since the publication of these time series studies, the number of sites directly measuring non-growing-season NEE (via eddy covariance or chambers) has more than doubled, capturing critical autumn, winter and springtime dynamics¹⁸. These more recent ground-based estimates suggest that non-growing-season CO_2 losses are currently higher than process model estimates of growing-season CO_2 uptake and are expected to increase in coming decades¹⁹. However, estimates of recent decadal NEE trends vary considerably depending on the modelling approach, especially in the permafrost zone^{20–22}. Thus, a comprehensive time

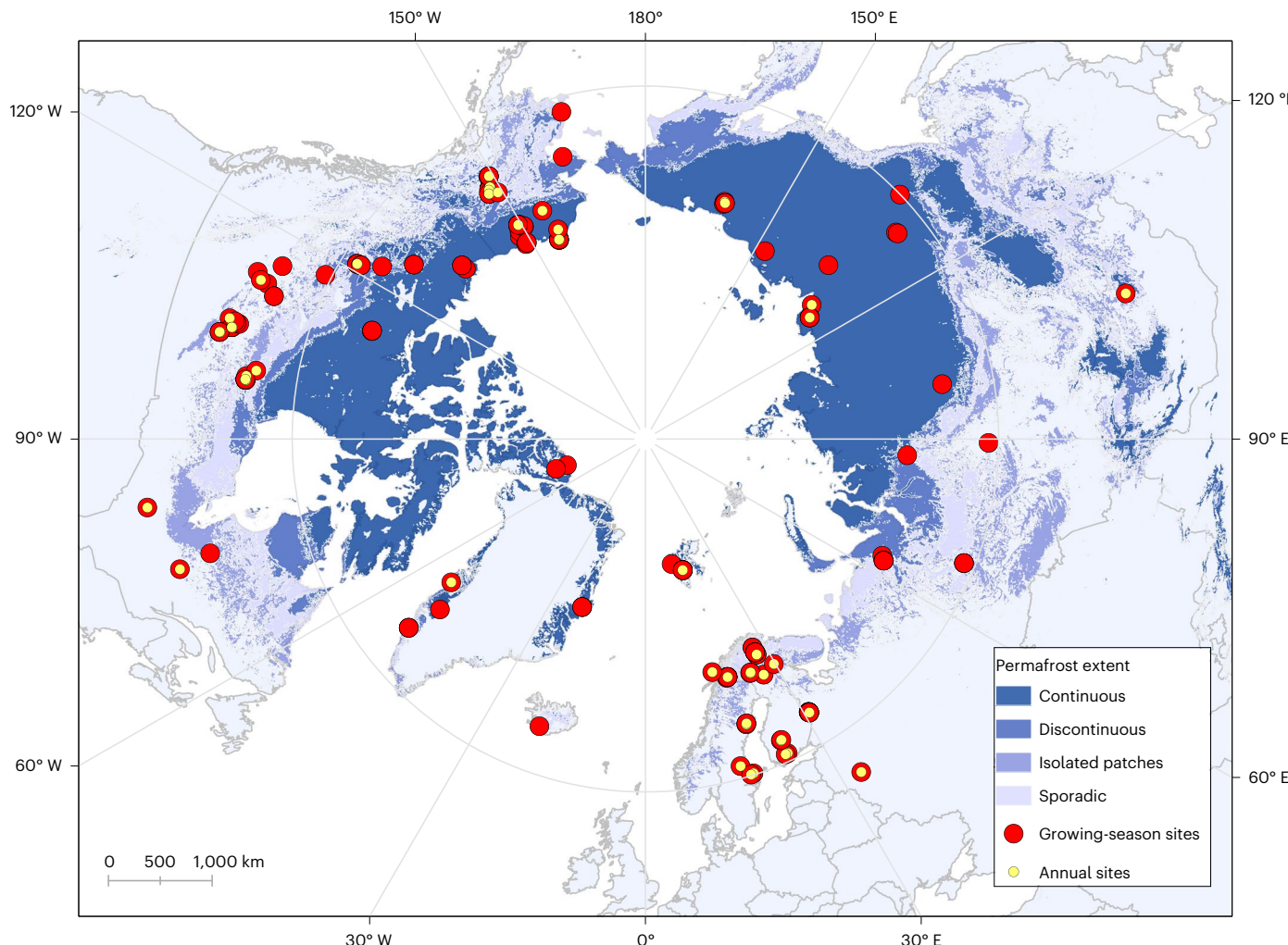


Fig. 1 | Distribution of sites containing summer (June–August) and annual CO₂ flux measurements across tundra and boreal forest ecosystems. Figure reproduced with permission from ref. 51, Elsevier.

series analysis of ground-based, annual measurements is needed to help constrain recent trajectories in the CO₂ balance of ecosystems across this rapidly warming region.

Although climate warming is probably contributing to an amplification of the annual C cycle of northern ecosystems, field-based observations of the C-cycle response to interannual temperature anomalies remain empirically unexplored. Direct temperature limitation of plant and microbial metabolism is well documented globally^{23,24} and is exacerbated under high-latitude growing-season conditions^{23,25–27}. However, evidence from warming experiments reveals that the responses of GPP and R_{eco} to temperature are rarely of equal magnitude, resulting in variable effects of temperature on NEE across ecosystems^{28–31}. This is partially because GPP and R_{eco} are constrained by additional resources that limit plant and microbial processes and mediate their temperature response^{32–34}. Water and nitrogen (N) availability are expected to limit both productivity and decomposition in ecosystems as temperature and CO₂ concentrations continue to rise^{26,34–38}, collectively influencing the NEE response to temperature³⁴. Consequently, the magnitude of the GPP and R_{eco} response to temperature is expected to vary with the local resource limitations of plant and microbial communities, resulting in differential impacts on net CO₂ balance across sites³⁴. Thus, an empirical understanding of how resource availability dictates the temperature response of NEE across ecosystems will be critical to constraining future projections under warming^{34,39–44}.

Here we present a comprehensive time series analysis of CO₂ flux observations across ecosystems within the tundra and boreal biomes, including the first analysis of full-year (annual) NEE observations. Our objectives were to (1) describe differences in decadal trends of NEE, GPP and R_{eco} between permafrost and non-permafrost ecosystems at the growing season and annual scale; and (2) determine how ecosystem-level factors such as permafrost presence, biome type, water balance and N availability affect the interannual C-cycle response to temperature across these ecosystems.

Long-term trends in C fluxes

We analysed decadal trends and drivers of interannual variability based on available data containing 6,741 monthly fluxes from 349 sites (1989–2022), 672 summer growing-season fluxes (June, July and August) from 181 sites (1992–2022) and 302 annual fluxes across 70 sites (1995–2022) (Fig. 1 and Supplementary Fig. 1). Most of these data are included in the ABCflux dataset⁴⁵, with some additional aggregate estimates from other sites (Methods and Supplementary Tables 1 and 2). To explore decadal trends in aggregate CO₂ fluxes over time, we fit a series of linear mixed-effects models with year as a fixed effect, an autoregressive correlation structure (corCAR1), and random slopes and intercepts for each site^{9,46}.

During the 92 day summer (June–August), we found strong evidence for increased net CO₂ uptake (decreasing NEE) across the time series. Notably, the observed change in summer NEE was

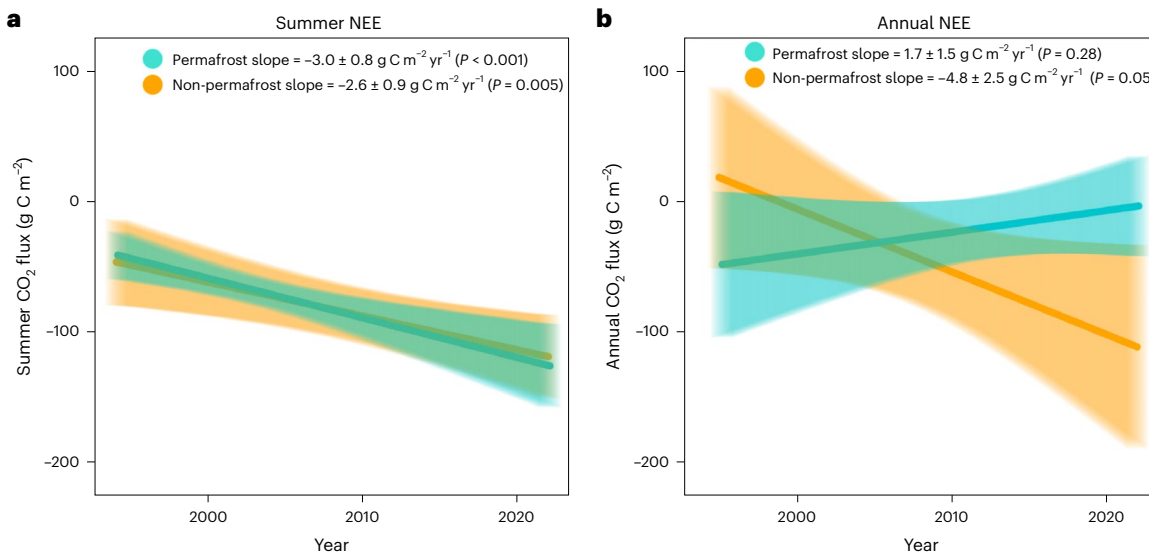


Fig. 2 | Slopes from linear mixed-effects models showing decadal changes in summer and annual NEE across high-latitude ecosystems. Slopes are reported \pm s.e., with error bands on the lines representing 95% confidence intervals. **a**, During the summer (June–August), permafrost and non-permafrost

ecosystems show similar decreases in NEE (increased land C uptake). **b**, Annual trends diverge, with non-permafrost sites showing a statistically significant decrease in NEE (greater C uptake) and permafrost sites trending towards increasing NEE (greater C losses) through time.

similar between ecosystems with permafrost ($-3.0 \pm 0.8 \text{ g C m}^{-2} \text{ yr}^{-1}$, conditional $R^2 (R^2_{\text{cond.}}) = 0.75, P < 0.001$; Fig. 2a) and those without ($-2.6 \pm 0.9 \text{ g C m}^{-2} \text{ yr}^{-1}, R^2_{\text{cond.}} = 0.79, P = 0.005$; Fig. 2a). However, the presence of permafrost led to a strong divergence in the annual (12 month) trends. Across non-permafrost ecosystems, the annual net CO₂ sink increased more than that in the summer alone, with annual NEE decreasing at a rate of $-4.8 \pm 2.4 \text{ g C m}^{-2} \text{ yr}^{-1}$ ($R^2_{\text{cond.}} = 0.79, P = 0.05$; Fig. 2b). In contrast, we did not detect a statistically significant trend in annual NEE across permafrost ecosystems, although the overall slope was positive (decreasing CO₂ sink, $1.7 \pm 1.5 \text{ g C m}^{-2} \text{ yr}^{-1}, P = 0.28$; Fig. 2b). This positive trend was statistically significant across North American permafrost sites ($3.7 \pm 1.7 \text{ g C m}^{-2} \text{ yr}^{-1}, R^2_{\text{cond.}} = 0.46, P < 0.05$; Supplementary Table 4), which encompassed 82% of our annual permafrost observations. These diverging annual trends highlight large differences in the trajectories of non-summer (September–May) CO₂ losses, which are offsetting increased summer gains in permafrost ecosystems but not non-permafrost ecosystems.

Decadal trends in both GPP and R_{eco} revealed clear amplification of the annual C cycle across permafrost ecosystems, with non-significant trends observed in the same direction but with greater variability across non-permafrost ecosystems (Fig. 3). In permafrost ecosystems, R_{eco} increased at a rate of $3.1 \pm 1.1 \text{ g C m}^{-2} \text{ yr}^{-1}$ ($R^2_{\text{cond.}} = 0.83, P = 0.005$; Fig. 3b) during the summer and at a rate of $6.1 \pm 3.2 \text{ g C m}^{-2} \text{ yr}^{-1}$ ($R^2_{\text{cond.}} = 0.81, P = 0.06$; Fig. 3d) annually, suggesting that half the R_{eco} increases in these ecosystems occurred during non-summer months (September–May). Carbon uptake also increased in permafrost ecosystems, with summer GPP decreasing at a rate of $-6.8 \pm 2.1 \text{ g C m}^{-2} \text{ yr}^{-1}$ (negative scale, decreasing GPP denotes increasing land uptake; $R^2_{\text{cond.}} = 0.77, P = 0.001$; Fig. 3a) and annual GPP decreasing at a similar rate of $-6.3 \pm 2.9 \text{ g C m}^{-2} \text{ yr}^{-1}$ ($R^2_{\text{cond.}} = 0.89, P = 0.03$; Fig. 3c). Thus, greater increases in productivity than respiration led to an increased summer CO₂ sink in permafrost ecosystems (Fig. 2a), supporting the idea that increasing non-summer R_{eco} is responsible for shifting permafrost systems towards an annual CO₂ source^{19,47} (Fig. 2b). Conversely, we found less evidence for a consistent amplification of GPP or R_{eco} across non-permafrost ecosystems (Fig. 3), despite net increases in summer and annual CO₂ uptake (decreasing NEE; Fig. 2). Interestingly, this suggests that rates of GPP are increasing relative to R_{eco} in non-permafrost sites where both fluxes are increasing, but also that the ratio of GPP

to R_{eco} may be increasing in sites where both fluxes are declining or remaining relatively stable through time.

An analysis of monthly flux trends revealed further evidence that permafrost ecosystems are experiencing greater amplification of the CO₂ cycle than non-permafrost ecosystems (Fig. 4 and Supplementary Table 6). Generally, NEE during summer months (June–August) trended towards greater CO₂ uptake (negative NEE slopes), with greater CO₂ release (positive NEE slopes) in the autumn and early winter (Fig. 4a). We found much stronger evidence for increased GPP and R_{eco} across permafrost ecosystems (Fig. 4b,c), consistent with the greater amplification we observed in summer and annual fluxes. September GPP gains in permafrost ecosystems suggest a lengthening growing season (Fig. 4b) but this increased late-growing-season CO₂ uptake was accompanied by increased respiratory CO₂ losses (Fig. 4c), leading to little change in September NEE (Fig. 4a). Critically, increases in R_{eco} in permafrost ecosystems extended into early winter (October–December; Fig. 4c), suggesting that deeper summer thaw is enhancing soil decomposition after plants become dormant and offsetting summer GPP gains^{19,20,47,48} (Figs. 2 and 4a).

Drivers of temperature effects on summer C flux

To assess how interannual variation in summer air temperature influenced summer CO₂ exchange across sites, we used a meta-regression approach to characterize how environmental factors affect the relationship between temperature and CO₂ fluxes. This analysis was independent of our time series analysis and instead focused directly on environmental controls over the relationship between temperature and C cycling. For each site with ≥ 5 years of data (Supplementary Fig. 1 and Supplementary Table 7), we calculated standardized slopes describing the relationship between temperature anomaly and CO₂ flux anomaly during the summer (June–August). We then used these temperature–flux slopes as dependent variables in separate variance-weighted regressions, with permafrost presence, biome type and soil C:N ratio as categorical predictors (Methods). To assess the effect of summer water availability across sites, we calculated an index of summer water use as the difference in millimetres between the 30 year mean summer actual evapotranspiration (AET_{summer}) and mean summer annual precipitation (MAP_{summer}) and used it as a predictor variable. Here, sites with positive values are less reliant on precipitation for their summer water

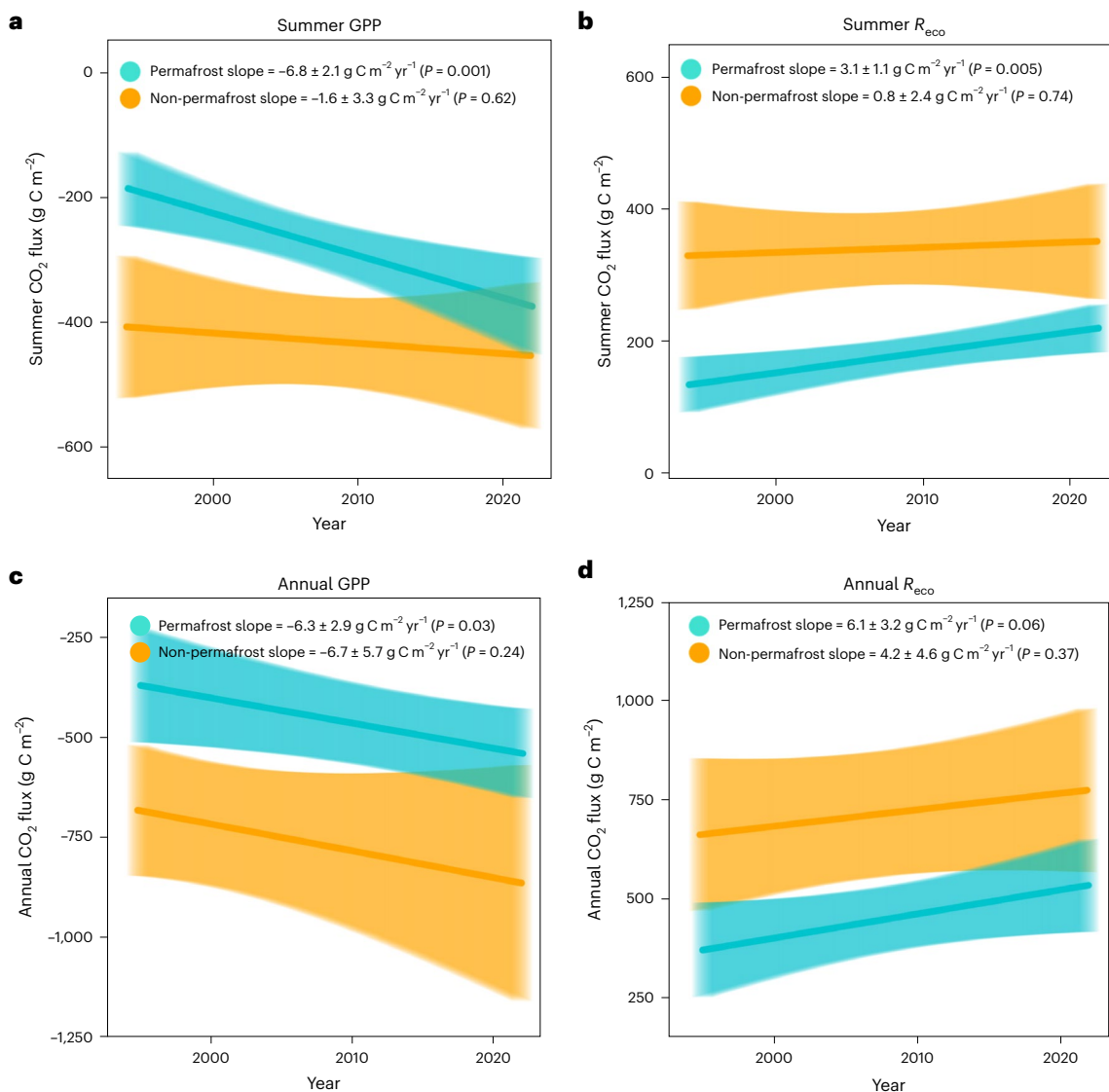


Fig. 3 | Decadal trends of summer annual GPP and R_{eco} . Slopes are reported \pm s.e., with error bands on lines representing 95% confidence intervals. **a, b**, Rates of summer (June–August) GPP (**a**) and R_{eco} (**b**) increased significantly and at a much greater rate in permafrost sites (green) than non-permafrost sites (orange),

highlighting a greater amplification of the C cycle over time in these ecosystems. **c, d**, Estimates of annual GPP (**c**) and R_{eco} (**d**) show similar trends but with greater uncertainty due to a lower number of annual observations.

use, probably due to the presence of a high water table and subsidies from snow-melt. Climate variables and soil C:N ratio were derived using the TerraClimate⁴⁹ and SoilGrids⁵⁰ datasets. Site-based permafrost presence was confirmed by site investigators or based on the TTOP model^{51,52} when site-based information was unavailable.

We did not find strong evidence that the temperature response of NEE differed between permafrost and non-permafrost ecosystems ($P = 0.14$) but non-permafrost ecosystems had a more consistently positive relationship between NEE and air temperature anomaly (lower-than-average CO₂ uptake in warmer-than-average summers; $P = 0.08$; Fig. 5a, top). Similarly, we did not find strong evidence that the temperature response of NEE differed by biome ($P = 0.15$; Fig. 5a, middle) but boreal forest ecosystems tended to have a positive relationship between NEE and summer temperatures (decreased summer CO₂ sink in warmer years; $P = 0.10$; Fig. 5a, middle), whereas tundra ecosystems showed both positive and negative relationships. In contrast, the effects of temperature on GPP and R_{eco} were more uniform regardless of permafrost presence or biome. Warmer summers consistently led to both higher plant CO₂ uptake (GPP negative scale, $P = 0.04$ across

all sites; Fig. 5b, top and middle) and respiratory CO₂ losses ($P < 0.001$ across all sites; Fig. 5c, top and middle). Thus, warmer years consistently amplified the summer C cycle (GPP and R_{eco}) but the combined effect of this amplification on CO₂ balance (NEE) was more variable across ecosystems.

Although warmer summers tended to have both higher GPP and R_{eco} , soil C:N ratio (calculated on a mass basis) emerged as a dominant constraint over this temperature amplification of the summer C cycle. This finding was present when the C:N ratio was used as a categorical (Fig. 5b,c, bottom) and as a continuous predictor variable (Extended Data Fig. 1 and Methods). In putatively N-poor ecosystems (C:N ratio > 15 in surface soils, below which microbial N-use efficiency has been shown to drop precipitously⁵³), warmer growing seasons led to higher GPP (increased CO₂ uptake, GPP negative scale; Fig. 5b, bottom) and R_{eco} (increased CO₂ losses; Fig. 5c, bottom). Interestingly, these relationships were opposite in more N-rich sites, where both GPP and R_{eco} tended to be lower than average during warmer years (Fig. 5b,c, bottom). Although relationships of fluxes with temperature were not consistently negative across all N-rich ecosystems ($P = 0.08$

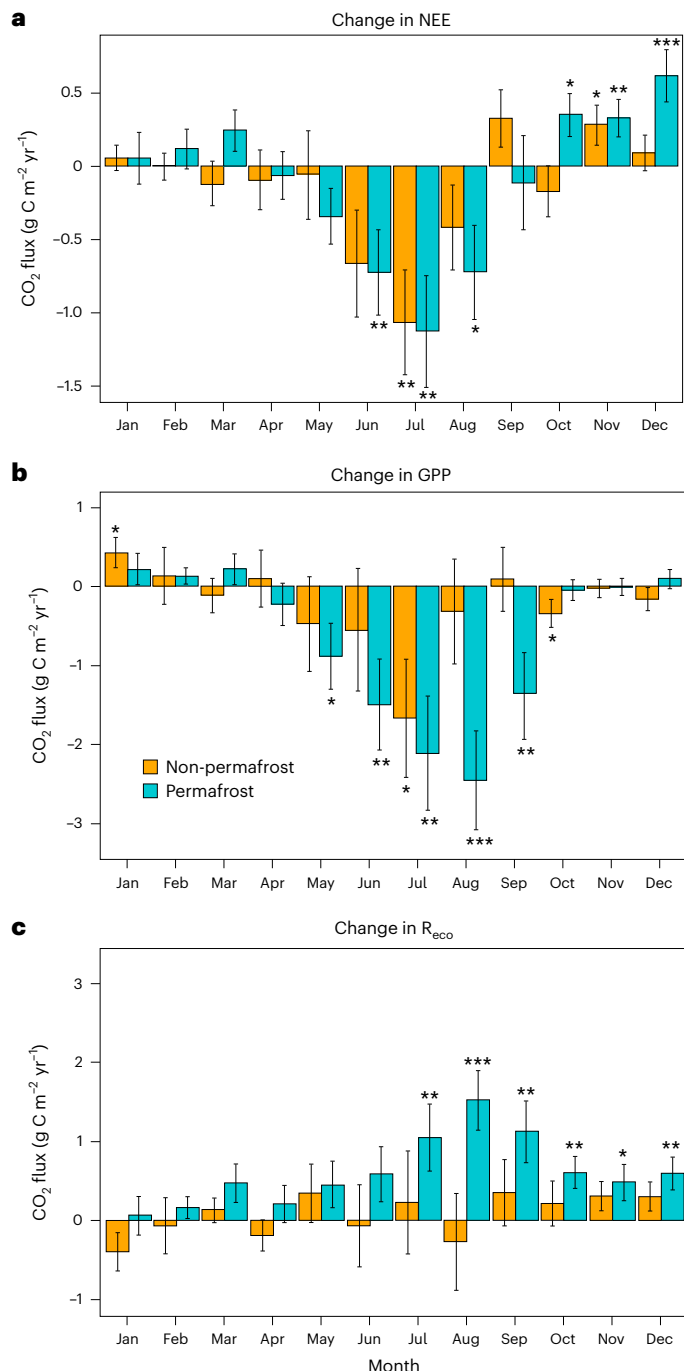


Fig. 4 | Decadal changes in NEE, GPP and R_{eco} by month. **a–c.** The monthly CO_2 flux changes in NEE (a), GPP (b) and R_{eco} (c) are shown. The y axis reflects the slope of change over time based on linear mixed-effects models with a random effect for site. Positive slope values indicate increasing NEE over time (decreasing net CO_2 uptake) and negative slope values indicate decreasing NEE over time (increasing net CO_2 uptake). Negative GPP slopes represent increasing productivity (CO_2 uptake), and positive R_{eco} slopes represent increasing respiratory losses to the atmosphere. Error bars reflect the s.e. for each slope. Asterisks denote statistical significance of the slopes not adjusted for multiple comparisons: * $P \leq 0.05$, ** $P \leq 0.01$, *** $P \leq 0.001$. Model parameters can be found in Supplementary Table 6.

for GPP, $P = 0.28$ for R_{eco}), they differed strongly from the uniformly positive temperature responses observed across more N-limited ecosystems ($P < 0.001$ for both GPP and R_{eco}). Interestingly, although soil C:N ratio strongly affected the magnitude and direction of the GPP and

R_{eco} response to warmer summers, it did not consistently predict the response of net C balance (NEE).

Beyond soil N availability, we found evidence that water availability also controlled the C-cycle response to temperature across ecosystems. In many permafrost ecosystems, water is perched near the soil surface on the thaw front, which prevents downward drainage, providing a source of near-surface summer water beyond rainfall. Ecosystems that regularly used water in excess of summer precipitation (long-term mean $\text{AET}_{\text{summer}}$ was greater than $\text{MAP}_{\text{summer}}$) showed higher-than-average GPP ($R^2 = 0.09, P = 0.05$; Fig. 6b) and R_{eco} ($R^2 = 0.16, P = 0.008$; Fig. 6c) during warm years. As the mean and interannual variability of summer GPP at most sites (mean = $-356 \text{ g C m}^{-2} \text{ yr}^{-1}$, s.d. = $71 \text{ g C m}^{-2} \text{ yr}^{-1}$) was greater than R_{eco} (mean = $269 \text{ g C m}^{-2} \text{ yr}^{-1}$, s.d. = $51 \text{ g C m}^{-2} \text{ yr}^{-1}$), the similar relative temperature sensitivity of these processes also resulted in some evidence for higher-than-average CO_2 uptake (lower NEE) in warm years at sites that were less reliant on summer precipitation for water use ($R^2 = 0.07, P = 0.07$; Fig. 6a). Both $\text{MAP}_{\text{summer}}$ and $\text{AET}_{\text{summer}}$ were individually correlated with a positive NEE response to temperature (higher-than-average NEE in warm years; Extended Data Fig. 2) across ecosystems but did not consistently affect GPP or R_{eco} .

Historically, high-latitude ecosystems have served as net annual C sinks for millennia^{54–56}. We found strong evidence that net summer CO_2 uptake has increased across these ecosystems in recent decades, with similar trends in permafrost and non-permafrost ecosystems. However, trends in non-summer months led to a strong divergence in the annual CO_2 budgets of these ecosystems (Fig. 2b). In non-permafrost ecosystems, the annual net CO_2 sink increased more than during the summer alone, suggesting that longer growing seasons are increasing annual plant uptake relative to respiration. By contrast, non-summer respiratory losses negated summer gains in permafrost ecosystems, leading to no detectable increase in the annual CO_2 sink (Figs. 2 and 3). Previous ground-based syntheses have suggested that permafrost ecosystems may have represented a net CO_2 source in recent decades^{9,19}, with non-growing-season CO_2 losses increasing over time^{9,19,31}, but have been unable to directly detect these changes due to data scarcity. Our analysis of an expanded dataset suggests that permafrost ecosystems may have remained neutral or a small net CO_2 sink in recent decades but provides empirical evidence that increased non-growing-season CO_2 losses have negated increases in summer CO_2 uptake.

Importantly, the site-level observations included in our analysis do not evenly represent the distribution of these ecosystems across high latitudes (Fig. 1), making it important to consider how these results scale globally¹⁸. Our results regarding permafrost ecosystems are largely driven by North American observations (where the annual sink appears to be decreasing; Supplementary Table 4), whereas the smaller number of annual observations from Eurasian ecosystems (20% of annual NEE observations; Supplementary Table 2) limit the inference regarding past trajectories using data from this region alone. This highlights the urgent need for increased ground-based monitoring of these critical landscapes¹⁸. By contrast, trends in non-permafrost ecosystems may be more strongly driven by observations from Eurasia^{11,21}, where trends were more consistent than in North America based on subset analyses (Supplementary Table 4) and both land masses were equally represented (51% North American and 49% Eurasian for annual NEE observations; Supplementary Table 2). The divergent annual NEE trajectories with permafrost presence in our data are largely in line with recent trends produced by satellite-driven, process-based models²¹, although they run contrary to those produced by atmospheric inversion models²⁰. Cross-validation of our models using a leave-one-out approach (that is, iteratively removing one site at a time and refitting models), and refitting the time series models in a Bayesian framework, suggested that conclusions surrounding changes in NEE were relatively robust but that trends in GPP and R_{eco} were more likely subject to greater biases due to site inclusion (Methods and Supplementary Table 5).

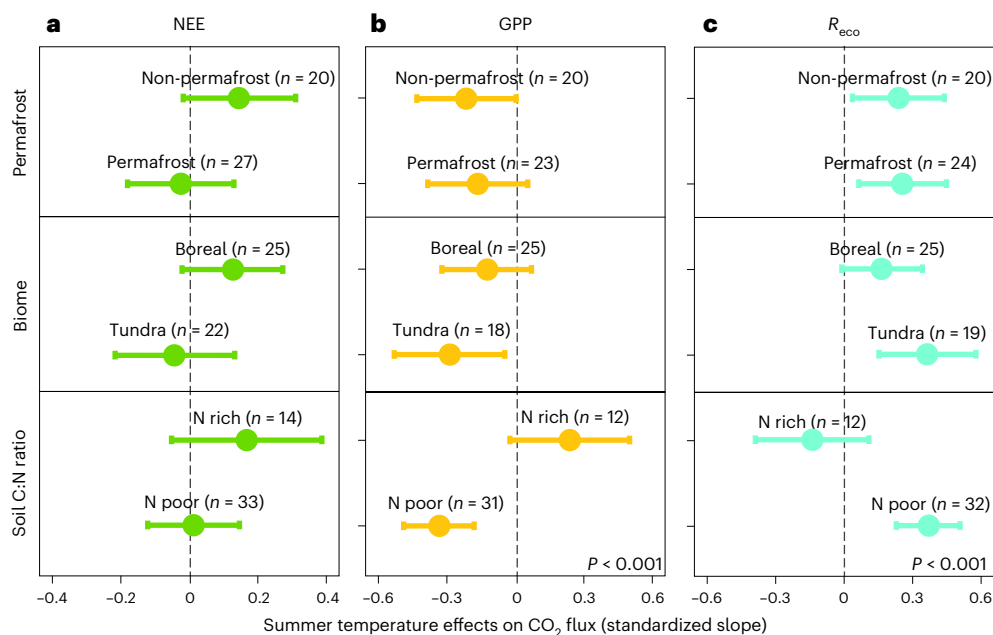


Fig. 5 | Site factors predicting the summer CO₂ flux response to summer air temperature. **a–c.** Results from linear regressions of the effects of ecosystem factors (permafrost presence (top), biome (middle) and soil C:N ratio (bottom)) on the relationship between summer air temperature and summer NEE (a), GPP (b) and R_{eco} (c). Standardized slopes reflect the effect of 1 s.d. (z-score) of summer temperature on C flux (also in units of s.d.). Error bars denote 95% confidence intervals, indicating consistent positive or negative relationships when not

overlapping with the dashed zero line. Sample sizes (n = number of sites) are presented above each bar for each group. On average, both GPP (negative scale; **b**, top) and R_{eco} (**c**, top) increase in warmer years regardless of permafrost presence but markedly less so in N-rich (soil C:N ratio < 15) systems, which have significantly lower rates of both CO₂ uptake and release during warmer years (**b**, bottom; **c**, bottom).

Thus, although this work represents an extensive time series analysis of annual flux measurements from northern ecosystems, it is critical to acknowledge the historical spatial biases present in the dataset.

The interannual NEE trends we observed underscore a rapid amplification of the C cycle in permafrost ecosystems^{9–13}. The presence of permafrost contributes to a short window for plant and microbial activity⁵⁷, leading to greater sensitivity to global change factors (for example, warming, CO₂ fertilization and nutrient feedbacks). Our time series shows decadal amplification of both summer GPP and R_{eco} across permafrost ecosystems (Figs. 3 and 4), with GPP effects dominating during the summer months and leading to increasing net CO₂ uptake during this time (Fig. 2a). Critically, early winter (October–December) CO₂ losses have also increased markedly in permafrost ecosystems (Fig. 4c), presumably due to warming-induced deepening of the active layer (thawed soil)^{58,59}, which lengthens the period for microbial decomposition of soil C⁶⁰. Here, increased late-season CO₂ losses offset summer C gains, resulting in little detectable change in the average annual budget across permafrost systems (Fig. 2b), with some indication of a shift towards C neutrality or future net C release. By contrast, decadal trends of increasing GPP and R_{eco} were less consistent (more variable) across non-permafrost ecosystems but their combined changes have resulted in an increased net annual C sink (Fig. 2b).

Summer water use emerged as an important control over the magnitude and direction of the summer C-cycle response to temperature across northern ecosystems^{14,61}. Ecosystems that regularly use soil water in excess of summer precipitation (30 year AET_{summer} > MAP_{summer}) responded to warmer summers with both higher productivity and respiration, suggesting that plants and microbes may be better able to take advantage of increased temperatures where summertime water subsidies (for example, perched surface water) are more available^{29,61,62}. This temperature amplification of GPP and R_{eco} largely cancelled out in these systems, resulting in only a weak trend towards an increased net summer CO₂ sink in warmer years (lower NEE; Fig. 6a). Conversely,

sites with higher total MAP_{summer} and AET_{summer} (greater absolute rates of water exchange) showed a significantly reduced summer CO₂ sink (higher NEE) in warm years, despite no consistent effects on the temperature sensitivity of GPP or R_{eco} alone (Supplementary Fig. 2). These higher-precipitation sites were largely non-permafrost landscapes that may lack perched surface water and be more closely tied to timing and availability of summer precipitation, consistent with positive correlations between precipitation and NEE at high latitudes³¹. High-latitude precipitation patterns are expected to change markedly along with temperatures over the next century^{63,64}. Our results suggest that the net changes in precipitation versus evapotranspiration, rather than these variables individually, may ultimately determine the GPP and R_{eco} (and together the NEE) response to warmer summer temperatures across these ecosystems. It also highlights C-cycle dynamics in ecosystems that access perched soil water that is likely to change, with access decreasing as permafrost degrades in a warmer world⁶⁵.

Our results further point to N limitation as an important control over temperature amplification of the summer C cycle in northern ecosystems, with more N-rich (lower C:N ratio) soils showing a diminished GPP and R_{eco} response to temperature. Soil C:N ratio is the dominant control over the temperature sensitivity of microbial respiration (Q_{10}) globally, with decomposition being more sensitive to temperature in soils with a higher C:N ratio, particularly in permafrost ecosystems^{25,66}. This causes N mineralization⁶⁷ and productivity⁶⁸ to be more temperature sensitive, ultimately leading to a greater temperature response of GPP and R_{eco} in more N-limited soils (Fig. 5b,c, bottom). Conversely, the soil microbial response to temperature is more muted in soils with a lower C:N ratio²⁵ and plant productivity is more likely to be limited by resources and stressors that are positively, negatively or neutrally related to temperature^{61,69–73}. Our findings imply that long-term increases in summer temperatures may lead to an amplification of the C cycle in more N-limited ecosystems. The impacts of warming may be less consistent in more N-rich ecosystems, potentially decelerating the

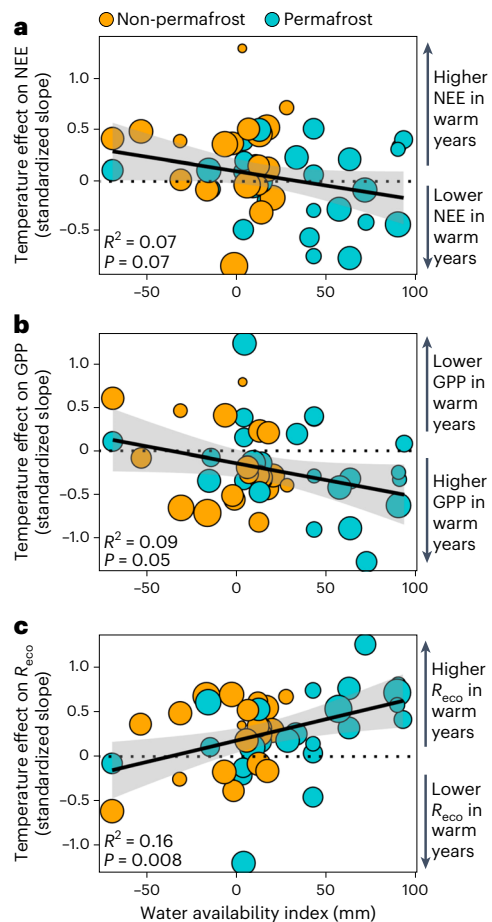


Fig. 6 | Effects of summer water use on summer CO₂ flux response to air temperature. a–c, Lines reflect linear regressions of the effects of summer water availability (xaxis, 30 year mean AET_{summer} minus 30-year MAP_{summer}) on the relationship between summer air temperature and NEE (a), GPP (b) and R_{eco} (c). Standardized slopes reflect the effect of 1 s.d. (z-score) of summer temperature on 1 s.d. of summer C flux. Positive x-axis values indicate sites where summer water use regularly exceeds precipitation inputs and near-surface soil water may be especially important. Points above the dashed zero line on the y axis represent sites where higher-than-average summer temperatures lead to higher-than-average NEE (a) and R_{eco} (c), or lower-than-average GPP (b). Larger points indicate greater confidence in the slope for each site and reflect model weights. Error bands represent 95% confidence intervals.

C cycle in ecosystems where temperature effects are driven by other factors (for example, soil drying and herbivory). Understanding these dynamics will be particularly important in permafrost ecosystems where large (currently unavailable) stocks of N may enter actively cycling N pools with increased thaw^{74–77}.

In summary, our decadal analysis of annual, ground-based measurements shows significant amplification of the C cycle across permafrost ecosystems. Increased respiration from permafrost soils during the non-growing season is probably causing these ecosystems to become a decreasing CO₂ sink (increasing NEE), despite concurrent increases in summer CO₂ uptake. Conversely, combined changes in GPP and R_{eco} have led to decadal increases in the net CO₂ sink (decreasing NEE) across non-permafrost ecosystems. Critically, temperature increases over the next century will coincide with large regional changes in both precipitation and N availability, particularly in permafrost ecosystems^{63,64,74,77}. Our results suggest that although greater N availability may initially increase rates of ecosystem C cycling^{78–80}, the long-term effects of N enrichment may result in reduced sensitivity of the C cycle (GPP and R_{eco}) to warmer summer temperatures^{68,81–83}.

Similarly, our results suggest that temperature-induced amplification of summer GPP and R_{eco} will be constrained by water availability, with greater rates of temperature-induced amplification occurring in sites that are less reliant on summer precipitation for water use^{61,84}. These findings provide empirical evidence that changing conditions in the permafrost region are affecting the trajectory of annual C dynamics in ecosystems within the tundra and boreal biomes^{3,9,15,19} and suggest that local resource availability will constrain the C-cycle response to warming across this region^{34,42,61,79}.

Online content

Any methods, additional references, Nature Portfolio reporting summaries, source data, extended data, supplementary information, acknowledgements, peer review information; details of author contributions and competing interests; and statements of data and code availability are available at <https://doi.org/10.1038/s41558-024-02057-4>.

References

1. Goldstein, A. et al. Protecting irrecoverable carbon in Earth's ecosystems. *Nat. Clim. Change* **10**, 287–295 (2020).
2. Olson, D. M. et al. Terrestrial ecoregions of the world: a new map of life on earth: a new global map of terrestrial ecoregions provides an innovative tool for conserving biodiversity. *BioScience* **51**, 933–938 (2001).
3. Schuur, E. A. G. et al. Permafrost and climate change: carbon cycle feedbacks from the warming Arctic. *Annu. Rev. Environ. Resour.* **47**, 343–371 (2022).
4. Hugelius, G. et al. Estimated stocks of circumpolar permafrost carbon with quantified uncertainty ranges and identified data gaps. *Biogeosciences* **11**, 6573–6593 (2014).
5. Turetsky, M. R. et al. Carbon release through abrupt permafrost thaw. *Nat. Geosci.* **13**, 138–143 (2020).
6. Rantanen, M. et al. The Arctic has warmed nearly four times faster than the globe since 1979. *Commun. Earth Environ.* **3**, 168 (2022).
7. Previdi, M., Smith, K. L. & Polvani, L. M. Arctic amplification of climate change: a review of underlying mechanisms. *Environ. Res. Lett.* **16**, 093003 (2021).
8. Natali, S. M. et al. Permafrost carbon feedbacks threaten global climate goals. *Proc. Natl Acad. Sci. USA* **118**, 2100163118 (2021).
9. Belshe, E. F., Schuur, E. A. G. & Bolker, B. M. Tundra ecosystems observed to be CO₂ sources due to differential amplification of the carbon cycle. *Ecol. Lett.* **16**, 1307–1315 (2013).
10. Jeong, S.-J. et al. Accelerating rates of Arctic carbon cycling revealed by long-term atmospheric CO₂ measurements. *Sci. Adv.* **4**, eaao1167 (2018).
11. Lin, X. et al. Siberian and temperate ecosystems shape Northern Hemisphere atmospheric CO₂ seasonal amplification. *Proc. Natl Acad. Sci. USA* **117**, 21079–21087 (2020).
12. Hu, L. et al. COS-derived GPP relationships with temperature and light help explain high-latitude atmospheric CO₂ seasonal cycle amplification. *Proc. Natl Acad. Sci. USA* **118**, e2103423118 (2021).
13. Zhang, Y. et al. Future reversal of warming-enhanced vegetation productivity in the Northern Hemisphere. *Nat. Clim. Change* **12**, 581–586 (2022).
14. Virkala, A.-M. et al. Statistical upscaling of ecosystem CO₂ fluxes across the terrestrial tundra and boreal domain: regional patterns and uncertainties. *Glob. Change Biol.* **27**, 4040–4059 (2021).
15. Braghieri, R. K. et al. Tipping point in North American Arctic-boreal carbon sink persists in new generation Earth system models despite reduced uncertainty. *Environ. Res. Lett.* **18**, 025008 (2023).
16. López-Blanco, E. et al. Evaluation of terrestrial pan-Arctic carbon cycling using a data-assimilation system. *Earth Syst. Dyn.* **10**, 233–255 (2019).

17. McGuire, A. D. et al. An assessment of the carbon balance of Arctic tundra: comparisons among observations, process models, and atmospheric inversions. *Biogeosciences* **9**, 3185–3204 (2012).

18. Pallandt, M. M. T. A. et al. Representativeness assessment of the pan-Arctic eddy covariance site network and optimized future enhancements. *Biogeosciences* **19**, 559–583 (2022).

19. Natali, S. M. et al. Large loss of CO_2 in winter observed across the northern permafrost region. *Nat. Clim. Change* **9**, 852–857 (2019).

20. Liu, Z. et al. Respiratory loss during late-growing season determines the net carbon dioxide sink in northern permafrost regions. *Nat. Commun.* **13**, 5626 (2022).

21. Watts, J. D. et al. Carbon uptake in Eurasian boreal forests dominates the high-latitude net ecosystem carbon budget. *Glob. Change Biol.* **29**, 1870–1889 (2023).

22. Wang, K. et al. Regional and seasonal partitioning of water and temperature controls on global land carbon uptake variability. *Nat. Commun.* **13**, 3469 (2022).

23. Huang, M. et al. Air temperature optima of vegetation productivity across global biomes. *Nat. Ecol. Evol.* **3**, 772–779 (2019).

24. Zhou, T., Shi, P., Hui, D. & Luo, Y. Global pattern of temperature sensitivity of soil heterotrophic respiration (Q_{10}) and its implications for carbon-climate feedback. *J. Geophys. Res. Biogeosci.* **114**, G02016 (2009).

25. Ren, S. et al. Higher temperature sensitivity of soil C release to atmosphere from northern permafrost soils as indicated by a meta-analysis. *Glob. Biogeochem. Cycles* **34**, e2020GB006688 (2020).

26. Hobbie, S. E., Schimel, J. P., Trumbore, S. E. & Randerson, J. R. Controls over carbon storage and turnover in high-latitude soils. *Glob. Change Biol.* **6**, 196–210 (2000).

27. Zhou, S. et al. Dominant role of plant physiology in trend and variability of gross primary productivity in North America. *Sci. Rep.* **7**, 41366 (2017).

28. Welker, J. M., Fahnestock, J. T., Henry, G. H. R., O'Dea, K. W. & Chimner, R. A. CO_2 exchange in three Canadian High Arctic ecosystems: response to long-term experimental warming. *Glob. Change Biol.* **10**, 1981–1995 (2004).

29. Oberbauer, S. F. et al. Tundra CO_2 fluxes in response to experimental warming across latitudinal and moisture gradients. *Ecol. Monogr.* **77**, 221–238 (2007).

30. Wu, Z., Dijkstra, P., Koch, G. W., Peñuelas, J. & Hungate, B. A. Responses of terrestrial ecosystems to temperature and precipitation change: a meta-analysis of experimental manipulation. *Glob. Change Biol.* **17**, 927–942 (2011).

31. Li, Z.-L. et al. Changes in net ecosystem exchange of CO_2 in Arctic and their relationships with climate change during 2002–2017. *Adv. Clim. Change Res.* **12**, 475–481 (2021).

32. Bloom, A. J., Chapin, F. S. & Mooney, H. A. Resource limitation in plants—an economic analogy. *Annu. Rev. Ecol. Syst.* **16**, 363–392 (1985).

33. Sinsabaugh, R. L., Manzoni, S., Moorhead, D. L. & Richter, A. Carbon use efficiency of microbial communities: stoichiometry, methodology and modelling. *Ecol. Lett.* **16**, 930–939 (2013).

34. Rastetter, E. B. et al. N and P constrain C in ecosystems under climate change: role of nutrient redistribution, accumulation, and stoichiometry. *Ecol. Appl.* **32**, e2684 (2022).

35. Zhu, Z. et al. Greening of the Earth and its drivers. *Nat. Clim. Change* **6**, 791–795 (2016).

36. Terrer, C. et al. A trade-off between plant and soil carbon storage under elevated CO_2 . *Nature* **591**, 599–603 (2021).

37. Reich, P. B., Hungate, B. A. & Luo, Y. Carbon–nitrogen interactions in terrestrial ecosystems in response to rising atmospheric carbon dioxide. *Annu. Rev. Ecol. Evol. Syst.* **37**, 611–636 (2006).

38. Aerts, R. The freezer defrosting: global warming and litter decomposition rates in cold biomes. *J. Ecol.* **94**, 713–724 (2006).

39. Le Noë, J. et al. Soil organic carbon models need independent time-series validation for reliable prediction. *Commun. Earth Environ.* **4**, 1–8 (2023).

40. Fisher, R. A. et al. Vegetation demographics in Earth system models: a review of progress and priorities. *Glob. Change Biol.* **24**, 35–54 (2018).

41. Wieder, W. R. et al. Beyond static benchmarking: using experimental manipulations to evaluate land model assumptions. *Glob. Biogeochem. Cycles* **33**, 1289–1309 (2019).

42. Braghieri, R. K. et al. Modeling global carbon costs of plant nitrogen and phosphorus acquisition. *J. Adv. Model. Earth Syst.* **14**, e2022MS003204 (2022).

43. Huntzinger, D. N. et al. Uncertainty in the response of terrestrial carbon sink to environmental drivers undermines carbon-climate feedback predictions. *Sci. Rep.* **7**, 4765 (2017).

44. Mevenkamp, H. et al. Reducing uncertainty of high-latitude ecosystem models through identification of key parameters. *Environ. Res. Lett.* **18**, 084032 (2023).

45. Virkkala, A.-M. et al. The ABCflux database: Arctic–boreal CO_2 flux observations and ancillary information aggregated to monthly time steps across terrestrial ecosystems. *Earth Syst. Sci. Data* **14**, 179–208 (2022).

46. Pinheiro, J., Bates, D. & R Core Team nlme: Linear and Nonlinear Mixed Effects Models. R version 3.1-164 <https://CRAN.R-project.org/package=nlme> (2023).

47. Commane, R. et al. Carbon dioxide sources from Alaska driven by increasing early winter respiration from Arctic tundra. *Proc. Natl Acad. Sci. USA* **114**, 5361–5366 (2017).

48. Parazoo, N. C., Koven, C. D., Lawrence, D. M., Romanovsky, V. & Miller, C. E. Detecting the permafrost carbon feedback: talik formation and increased cold-season respiration as precursors to sink-to-source transitions. *Cryosphere* **12**, 123–144 (2018).

49. Abatzoglou, J. T., Dobrowski, S. Z., Parks, S. A. & Hegewisch, K. C. TerraClimate, a high-resolution global dataset of monthly climate and climatic water balance from 1958–2015. *Sci. Data* **5**, 170191 (2018).

50. Poggio, L. et al. SoilGrids 2.0: producing soil information for the globe with quantified spatial uncertainty. *SOIL* **7**, 217–240 (2021).

51. Obu, J. et al. Northern Hemisphere permafrost map based on TTOP modelling for 2000–2016 at 1 km^2 scale. *Earth Sci. Rev.* **193**, 299–316 (2019).

52. Obu, J., Westermann, S., Kääb, A. & Bartsch, A. Ground temperature map, 2000–2016, Northern Hemisphere permafrost. PANGAEA <https://doi.org/10.1594/PANGAEA.888600> (2018).

53. Mooshammer, M. et al. Adjustment of microbial nitrogen use efficiency to carbon:nitrogen imbalances regulates soil nitrogen cycling. *Nat. Commun.* **5**, 3694 (2014).

54. Zech, R., Huang, Y., Zech, M., Tarozzo, R. & Zech, W. High carbon sequestration in Siberian permafrost loess-paleosols during glacials. *Climate* **7**, 501–509 (2011).

55. Jones, M. C. et al. Past permafrost dynamics can inform future permafrost carbon-climate feedbacks. *Commun. Earth Environ.* **4**, 272 (2023).

56. Schuur, E. A. G. et al. Vulnerability of permafrost carbon to climate change: implications for the global carbon cycle. *BioScience* **58**, 701–714 (2008).

57. El-Amine, M. et al. What explains the year-to-year variation in growing season timing of boreal black spruce forests? *Agric. For. Meteorol.* **324**, 109113 (2022).

58. Hicks Pries, C. E., Schuur, E. A. G. & Crummer, K. G. Thawing permafrost increases old soil and autotrophic respiration in tundra: partitioning ecosystem respiration using $\delta^{13}\text{C}$ and $\Delta^{14}\text{C}$. *Glob. Change Biol.* **19**, 649–661 (2013).

59. Nowinski, N. S., Taneva, L., Trumbore, S. E. & Welker, J. M. Decomposition of old organic matter as a result of deeper active layers in a snow depth manipulation experiment. *Oecologia* **163**, 785–792 (2010).

60. Biskaborn, B. K. et al. Permafrost is warming at a global scale. *Nat. Commun.* **10**, 264 (2019).

61. Zona, D. et al. Pan-Arctic soil moisture control on tundra carbon sequestration and plant productivity. *Glob. Change Biol.* **29**, 1267–1281 (2022).

62. Chivers, M. R., Turetsky, M. R., Waddington, J. M., Harden, J. W. & McGuire, A. D. Effects of experimental water table and temperature manipulations on ecosystem CO₂ fluxes in an Alaskan rich fen. *Ecosystems* **12**, 1329–1342 (2009).

63. Zhang, X. et al. Enhanced poleward moisture transport and amplified northern high-latitude wetting trend. *Nat. Clim. Change* **3**, 47–51 (2013).

64. McCrystall, M. R., Stroeve, J., Serreze, M., Forbes, B. C. & Screen, J. A. New climate models reveal faster and larger increases in Arctic precipitation than previously projected. *Nat. Commun.* **12**, 6765 (2021).

65. Rodenhizer, H. et al. Abrupt permafrost thaw drives spatially heterogeneous soil moisture and carbon dioxide fluxes in upland tundra. *Glob. Change Biol.* **29**, 6286–6302 (2023).

66. Haaf, D., Six, J. & Doetterl, S. Global patterns of geo-ecological controls on the response of soil respiration to warming. *Nat. Clim. Change* **11**, 623–627 (2021).

67. Liu, Y. et al. A global synthesis of the rate and temperature sensitivity of soil nitrogen mineralization: latitudinal patterns and mechanisms. *Glob. Change Biol.* **23**, 455–464 (2017).

68. Liu, Y., Men, M., Peng, Z., Houx, J. & Peng, Y. Nitrogen availability determines ecosystem productivity in response to climate warming. *Ecology* **103**, e3823 (2022).

69. Shaw, A. A. & Cleveland, C. C. The effects of temperature on soil phosphorus availability and phosphatase enzyme activities: a cross-ecosystem study from the tropics to the Arctic. *Biogeochemistry* **151**, 113–125 (2020).

70. Yu, Q., Epstein, H., Engstrom, R. & Walker, D. Circumpolar arctic tundra biomass and productivity dynamics in response to projected climate change and herbivory. *Glob. Change Biol.* **23**, 3895–3907 (2017).

71. Falk, J. M., Schmidt, N. M., Christensen, T. R. & Ström, L. Large herbivore grazing affects the vegetation structure and greenhouse gas balance in a high arctic mire. *Environ. Res. Lett.* **10**, 045001 (2015).

72. Sjögersten, S., van der Wal, R. & Woodin, S. J. Habitat type determines herbivory controls over CO₂ fluxes in a warmer Arctic. *Ecology* **89**, 2103–2116 (2008).

73. Chen, H. et al. Soil drying weakens the positive effect of climate factors on global gross primary production. *Ecol. Indic.* **129**, 107953 (2021).

74. Burke, E., Chadburn, S. & Huntingford, C. Thawing permafrost as a nitrogen fertiliser: implications for climate feedbacks. *Nitrogen* **3**, 353–375 (2022).

75. Norby, R. J., Sloan, V. L., Iversen, C. M. & Childs, J. Controls on fine-scale spatial and temporal variability of plant-available inorganic nitrogen in a polygonal tundra landscape. *Ecosystems* **22**, 528–543 (2019).

76. Lacroix, F. et al. Mismatch of N release from the permafrost and vegetative uptake opens pathways of increasing nitrous oxide emissions in the high Arctic. *Glob. Change Biol.* **28**, 5973–5990 (2022).

77. Strauss, J. et al. A globally relevant stock of soil nitrogen in the Yedoma permafrost domain. *Nat. Commun.* **13**, 6074 (2022).

78. Mack, M. C., Schuur, E. A. G., Bret-Harte, M. S., Shaver, G. R. & Chapin, F. S. Ecosystem carbon storage in arctic tundra reduce by long-term nutrient fertilization. *Nature* **431**, 440–443 (2004).

79. Hobbie, S. E., Nadelhoffer, K. J. & Högberg, P. A synthesis: the role of nutrients as constraints on carbon balances in boreal and arctic regions. *Plant Soil* **242**, 163–170 (2002).

80. López-Blanco, E. et al. The future of tundra carbon storage in Greenland—sensitivity to climate and plant trait changes. *Sci. Total Environ.* **846**, 157385 (2022).

81. Xiao, H. et al. Responses of soil respiration and its temperature sensitivity to nitrogen addition: a meta-analysis in China. *Appl. Soil Ecol.* **150**, 103484 (2020).

82. Peng, J. et al. Nitrogen enrichment alters climate sensitivity of biodiversity and productivity differentially and reverses the relationship between them in an alpine meadow. *Sci. Total Environ.* **835**, 155418 (2022).

83. Zhao, P. et al. Long-term nitrogen addition raises the annual carbon sink of a boreal forest to a new steady-state. *Agric. For. Meteorol.* **324**, 109112 (2022).

84. Helbig, M. et al. Warming response of peatland CO₂ sink is sensitive to seasonality in warming trends. *Nat. Clim. Change* **12**, 743–749 (2022).

Publisher's note Springer Nature remains neutral with regard to jurisdictional claims in published maps and institutional affiliations.

Open Access This article is licensed under a Creative Commons Attribution 4.0 International License, which permits use, sharing, adaptation, distribution and reproduction in any medium or format, as long as you give appropriate credit to the original author(s) and the source, provide a link to the Creative Commons licence, and indicate if changes were made. The images or other third party material in this article are included in the article's Creative Commons licence, unless indicated otherwise in a credit line to the material. If material is not included in the article's Creative Commons licence and your intended use is not permitted by statutory regulation or exceeds the permitted use, you will need to obtain permission directly from the copyright holder. To view a copy of this licence, visit <http://creativecommons.org/licenses/by/4.0/>.

© The Author(s) 2024

Craig R. See   **Anna-Maria Virkkala**  **Susan M. Natali**², **Brendan M. Rogers**  **Marguerite Mauritz**³, **Christina Biasi**  **Stef Bokhorst**  **Julia Boike**  **M. Syndonia Bret-Harte**  **Gerardo Celis**¹⁰, **Namyi Chae**¹¹, **Torben R. Christensen**  **Sara June Murner (Connon)**¹⁴, **Sigrid Dengel**¹⁵, **Han Dolman**^{16,17}, **Colin W. Edgar**  **Bo Elberling**¹⁸, **Craig A. Emmerton**  **Eugénie S. Euskirchen**  **Mathias Göckede**  **Achim Grelle**  **Liam Heffernan**¹⁷, **Manuel Helbig**  **David Holl**  **Elyn Humphreys**  **Hiroki Iwata**  **Järvi Järveoja**  **Hideki Kobayashi**  **John Kochendorfer**³¹, **Pasi Kolari**³², **Ayumi Kotani**³³, **Lars Kutzbach**  **Min Jung Kwon**^{20,25}, **Emma R. Lathrop**¹, **Efrén López-Blanco**  **Ivan Mammarella**  **Maija E. Marushchak**  **Mikhail Mastepanov**  **12,35**,

Yojiro Matsuura³⁶, Lutz Merbold³⁷, Gesa Meyer³⁸, Christina Minions³⁹, Mats B. Nilsson³⁹, Julia Nojeim³⁹, Steven F. Oberbauer⁴⁰, David Olefeldt⁴¹, Sang-Jong Park⁴², Frans-Jan W. Parmentier⁴³, Matthias Peichl³⁹, Darcy Peter^{2,44}, Roman Petrov⁴⁵, Rafael Poyatos^{46,47}, Anatoly S. Prokushkin⁴⁸, William Quinton⁴⁹, Heidi Rodenhizer², Torsten Sachs^{24,50}, Kathleen Savage², Christopher Schulze^{23,41}, Sofie Sjögersten⁵¹, Oliver Sonnentag²³, Vincent L. St. Louis¹⁹, Margaret S. Torn¹⁵, Eeva-Stiina Tuittila⁵², Masahito Ueyama⁵³, Andrej Varlagin⁵⁴, Carolina Voigt^{5,25}, Jennifer D. Watts², Donatella Zona⁵⁵, Viacheslav I. Zyryanov⁴⁸ & Edward A. G. Schuur¹

¹Center for Ecosystem Science and Society, Northern Arizona University, Flagstaff, AZ, USA. ²Woodwell Climate Research Center, Falmouth, MA, USA.

³University of Texas El Paso, El Paso, TX, USA. ⁴Department of Ecology, University of Innsbruck, Innsbruck, Austria. ⁵Department of Environmental and Biological Sciences, University of Eastern Finland, Kuopio, Finland. ⁶Department of Ecological Science, Vrije Universiteit Amsterdam, Amsterdam, The Netherlands. ⁷Alfred Wegener Institute, Helmholtz Centre for Polar and Marine Research, Potsdam, Germany. ⁸Humboldt Universität zu Berlin, Berlin, Germany. ⁹University of Alaska Fairbanks, Fairbanks, AK, USA. ¹⁰University of Arkansas, Fayetteville, AK, USA. ¹¹Institute of Life Science and Natural Resources, Korea University, Seoul, South Korea. ¹²Department of Ecosystems, Aarhus University, Roskilde, Denmark. ¹³Water, Energy and Environmental Engineering Research Unit, Oulu University, Oulu, Finland. ¹⁴Green Seal Environmental LLC, Sagamore Beach, MA, USA. ¹⁵Lawrence Berkeley National Laboratory, Berkeley, CA, USA. ¹⁶Royal Netherlands Institute for Sea Research, Texel, Netherlands. ¹⁷Department of Earth Sciences, Vrije Universiteit Amsterdam, Amsterdam, The Netherlands. ¹⁸Center for Permafrost (CENPERM), Department of Geosciences and Natural Resource Management, University of Copenhagen, Copenhagen, Denmark. ¹⁹Department of Biological Sciences, University of Alberta, Edmonton, Alberta, Canada. ²⁰Max Planck Institute for Biogeochemistry, Jena, Germany. ²¹Department of Forestry and Wood Technology, Linnaeus University, Växjö, Sweden. ²²Dalhousie University, Halifax, Nova Scotia, Canada. ²³Département de Géographie, Université de Montréal, Montreal, Quebec, Canada. ²⁴GFZ German Research Centre for Geoscience, Potsdam, Germany. ²⁵Institute of Soil Science, Universität Hamburg, Hamburg, Germany. ²⁶Center for Earth System Research and Sustainability (CEN), Universität Hamburg, Hamburg, Germany. ²⁷Carleton University, Ottawa, Ontario, Canada. ²⁸Department of Environmental Science, Shinshu University, Matsumoto, Japan. ²⁹Department of Forest Ecology and Management, Swedish University of Agricultural Sciences, Umeå, Sweden.

³⁰Japan Agency for Marine-Earth Science and Technology, Yokohama, Japan. ³¹ARL/ATDD, National Oceanic and Atmospheric Administration, Oak Ridge, TN, USA. ³²Institute for Atmospheric and Earth System Research/Physics, Faculty of Science, University of Helsinki, Helsinki, Finland. ³³Nagoya University, Nagoya, Japan. ³⁴Greenland Institute for Natural Resources, Nuuk, Greenland. ³⁵Oulanka Research Station, Oulu University, Kuusamo, Finland. ³⁶Forestry and Forest Products Research Institute, Tsukuba, Japan. ³⁷Research Division Agroecology and Environment, Agroscope, Zurich, Switzerland. ³⁸Climate Research Division, Environment and Climate Change Canada, Victoria, British Columbia, Canada. ³⁹Yale Center for Business and the Environment, New Haven, CT, USA. ⁴⁰Department of Biological Sciences and Institute of Environment, Florida International University, Miami, FL, USA. ⁴¹Department of Renewable Resources, University of Alberta, Edmonton, Alberta, Canada. ⁴²Korea Polar Research Institute, Incheon, South Korea. ⁴³Centre for Biogeochemistry of the Anthropocene, Department of Geosciences, University of Oslo, Oslo, Norway. ⁴⁴Alaska Conservation Foundation, Anchorage, AK, USA. ⁴⁵Institute for Biological Problems of Cryolithozone, Siberian Branch of the Russian Academy of Sciences, Yakutsk, Russia. ⁴⁶CRAEF, Cerdanyola del Vallès, Spain. ⁴⁷Universitat Autònoma de Barcelona, Cerdanyola del Vallès, Spain. ⁴⁸VN Sukachev Institute of Forest, Siberian Branch of the Russian Academy of Sciences, Akademgorodok, Russia. ⁴⁹Wilfrid Laurier University, Waterloo, Ontario, Canada. ⁵⁰Institute of Geobotany, Technische Universität Braunschweig, Braunschweig, Germany. ⁵¹University of Nottingham, Nottingham, UK. ⁵²School of Forest Sciences, University of Eastern Finland, Joensuu, Finland. ⁵³Graduate School of Agriculture, Osaka Metropolitan University, Osaka, Japan. ⁵⁴A. N. Severtsov Institute of Ecology and Evolution, Russian Academy of Sciences, Moscow, Russia. ⁵⁵Department of Biology, San Diego State University, San Diego, CA, USA.  e-mail: crsee@umn.edu

Methods

Data compilation

The majority of the data used in our analysis are published as the ABCflux database, which consists of monthly gap-filled estimates of NEE, GPP and R_{eco} ⁴⁵. As the primary objective of this work was to assess long-term trends in annual and summer fluxes, we included published fluxes reported at these timesteps, which were unable to be parsed into monthly timesteps (and therefore not suitable for inclusion in ABCflux). These additional aggregate fluxes were compiled during a working group through the US National Center for Ecological Analysis and Synthesis in 2019. After data cleaning, this resulted in 75 additional summer NEE fluxes across 12 sites, along with 50 and 51 summer fluxes of GPP and R_{eco} across 8 sites. At the annual timestep, this resulted in 29 additional annual NEE fluxes across 4 sites, and 22 annual fluxes of GPP and R_{eco} across 3 sites. Many of these additional aggregate fluxes were included in a recent upscaling study⁴⁴. Finally, more recent monthly observations that were unavailable when ABCflux was published (that is, observations after 30 September 2020) were solicited from site investigators during the Permafrost Carbon Network meeting in December 2021, with data accepted through the end of 2022. This resulted in 275 monthly NEE and GPP (and 299 R_{eco}) estimates not included in ABCflux, with 6 additional ecosystems represented and updated flux estimates for timeseries from 3 sites currently represented in ABCflux.

We calculated summer ecosystem fluxes of NEE, GPP and R_{eco} as the sum of June, July and August for sites with monthly data, without gap-filling (that is, all 3 months were required for inclusion). For summer fluxes incorporated from the literature, we standardized growing-season estimates to 92 days to make them comparable to the summer (June–August) calculated using ABCflux. Similarly, annual fluxes were calculated in ABCflux by summing NEE, GPP and R_{eco} across the 12 month calendar year (that is, January–December). We did not include years with missing months and, in the case of eddy covariance towers, only included annual estimates of GPP and R_{eco} when the site also had a full 12 months of NEE (required for GPP and R_{eco} calculations). The monthly NEE fluxes calculated in the ABCflux database were primarily (79%) measured using the eddy covariance method, with GPP and R_{eco} derived using the night-time partitioning method. ABCflux also includes NEE measured using chamber and diffusion methods (approximately 10–20 chambers per site), which include at least 3 temporal measurements per month for summer months (June–August) and at least 1 temporal replicate during non-summer months. Further details regarding the data coverage, limitations and uncertainties are described in the ABCflux data description⁴⁵. Our final dataset is summarized in Supplementary Tables 1 and 2.

For each site in our analysis, we used the TerraClimate database⁴⁹ to provide interannual estimates of summer air temperature (calculated as the 3 month mean of June, July and August) and precipitation and AET (calculated as the sum of June, July and August). We calculated the mean summertime water use for each site as the difference between 30 year mean evapotranspiration and precipitation. Permafrost presence and biome type (tundra or boreal) were reported by investigators or based on literature reports from the site. Sites where permafrost information was unavailable were categorized as permafrost when in the continuous or discontinuous zone based on the Permafrost Extent and Ground Temperature Map^{51,52}. Finally, we calculated the soil C:N ratio at each site based on estimates of C and N pools from the SoilGrids 2.0 dataset⁵⁰.

Time series analyses of decadal fluxes

An initial Akaike-information-criterion-based assessment of candidate linear mixed-effects models that included time, permafrost, biome and climatic variables (temperature, precipitation and evapotranspiration) revealed the consistent presence of permafrost-by-year interactions across the most parsimonious models (lowest Akaike information criterion). Climate, biome and permafrost presence are inherently

correlated across high-latitude ecosystems (the presence of permafrost requires mean annual temperatures $<0^{\circ}\text{C}$ for a minimum of 2 years) and this dataset was not designed to meaningfully parse these factors. Our primary goal was to assess long-term annual trends in NEE across permafrost ecosystems compared with non-permafrost ecosystems and so we chose a simplified, spatially agnostic approach to detecting change⁹. To test whether C fluxes were increasing through time, we analysed our compiled summer and annual estimates of NEE, GPP and R_{eco} as dependent variables in linear mixed-effects models (fit separately for permafrost and non-permafrost ecosystems), with measurement year as the fixed effect and random slopes and intercepts for each site. We applied an autoregressive variance structure (corCAR1) to all models to account for potential autocorrelation⁹. Model fits were assessed for normality and heteroscedasticity of residuals, with little effect of individual sites driving long-term trends across the dataset (Supplementary Fig. 2). In addition to annual and growing-season changes, we analysed trends in monthly fluxes but were unable to achieve model convergence for many months using our more restrictive model. For consistency, we analysed all monthly trends using a simplified model that included a random intercept (but not slope) for ecosystem and an uncorrelated within-group covariance structure.

Uncertainty and sensitivity analyses of time series models

As the number of sites collecting data has increased since the beginning of our time series, we re-ran our models on a subset of the data to assess the robustness of our findings to temporal biases in data collection. We re-ran the models on the subset of observations from 2003 to present, representing the most recent 20 years of data. This represents 85% and 81% of summer and annual NEE estimates, 87% and 74% of summer and annual GPP, and 85% and 81% of summer and annual R_{eco} estimates, respectively (Supplementary Table 3). Similarly, we subset our data by landmass and re-ran the models separately for North America (including Greenland) and Eurasia (Supplementary Table 4) to assess the effect of broad-scale spatial patterns in data collection on our results. North America (largely Alaska) represents 82% of our annual observations of permafrost NEE (Supplementary Table 2). To further assess the uncertainty in the slope estimates of our full time series models, we refit all models (with an identical random effects and autocorrelation structure) in a Bayesian framework using the brms package in R (Supplementary Table 5). For Bayesian models we assigned the fixed effect parameters from the frequentist model outputs as prior distributions, with relatively uninformative priors for the random effects and covariance parameters (Student's t ; degrees of freedom (v) = 3, location (μ) = 0, scale (σ) = 47) and Lewandowski–Kurowicka–Joe (shape (η) = 1) distributions, respectively), and then ran each time series model 8 separate Markov chain Monte Carlo chains, resulting in 64,000 total samples in the posterior distribution. We further assessed the robustness of the frequentist model findings using leave-one-out cross-validation based on cluster-wise exclusion using the cv package in R⁸⁵. Further descriptions of these analyses accompany the results in Supplementary Tables 3–5. Collectively, these additional analyses point to a greater degree of confidence in NEE time series than in GPP or R_{eco} time series (Supplementary Tables 3–5), perhaps due to the larger sample size for NEE observations (Supplementary Table 2).

Meta-regression of factors influencing summer C flux response to temperature

To assess how ecosystem characteristics affect the summer C-cycle response to temperature, we used a meta-regression approach. For each site in the dataset containing at least 5 years of summer data (June–August, $n = 47$ for NEE, $n = 43$ for GPP, $n = 44$ for R_{eco} ; Supplementary Table 6), we calculated standardized slopes for the relationship between summer temperature anomaly (in standard deviations from the 30 year mean) and C flux anomaly (in standard deviations from the interannual mean across available years). We used these

slopes and their associated errors as response variables in a series of variance-weighted regression models (that is, linear models weighted by inverse of site-level standard errors of temperature slopes). Predictor variables included permafrost presence, biome (boreal versus tundra), 30 year mean summer precipitation, 30 year mean AET_{summer}, mean summer water use (evapotranspiration minus precipitation) and soil C:N ratio.

As soil N availability in deeper horizons changes with thaw depth during the summer in permafrost systems, we chose to use the mass-based C:N ratio of surface soil (top 5 cm) as an index of relative plant N limitation across these ecosystems. Unlike climatic factors, which co-vary with ecosystems in this dataset, soil C:N ratio was less consistently related to permafrost or biome type across these sites (Supplementary Table 7). When used as a continuous predictor across ecosystems, we found evidence for soil C:N ratio effects on both GPP and R_{eco} response to temperature (Extended Data Fig. 1). However, the gridded product used to create these soil C:N ratio estimates is subject to considerable uncertainty across sites⁵⁰. Given the relatively small number of observations in our dataset, we chose to bin observations of soil C:N ratio using a threshold of >15 to denote N limitation (Fig. 5). We chose this threshold because it is slightly higher than the average C:N ratio of fungal biomass (approximately 13 on a mass basis⁸⁶), which dominates microbial biomass in high-latitude systems⁸⁷, but is still likely a conservative threshold for N limitation as microbial N use efficiency appears to increase with soil C:N ratio up to 20 (ref. 53).

Data availability

Monthly flux data are archived and freely available from the Oak Ridge National Laboratory Distributed Active Archive Center at https://daac.ornl.gov/cgi-bin/dsviewer.pl?ds_id=1934. Aggregated fluxes are available with code at Zenodo (<https://doi.org/10.5281/zenodo.10987900>)⁸⁸.

Code availability

Code associated with this work is archived at Zenodo (<https://doi.org/10.5281/zenodo.10987900>)⁸⁸.

References

85. Fox, J. & Monette, G. cv: Cross-Validation of regression models. R version 4.3.1 <https://CRAN.R-project.org/package=cv> (2024).
86. Zhang, J. & Elser, J. J. Carbon:nitrogen:phosphorus stoichiometry in fungi: a meta-analysis. *Front. Microbiol.* **8**, 1281 (2017).
87. He, L. et al. Global biogeography of fungal and bacterial biomass carbon in topsoil. *Soil Biol. Biochem.* **151**, 108024 (2020).
88. See, C. R. Decadal increases in carbon uptake offset by respiratory losses across northern permafrost ecosystems. Zenodo <https://doi.org/10.5281/zenodo.10987900> (2024).

Acknowledgements

This study was supported by funding to E.A.G.S. from the NSF PLR Arctic System Science Research Networking Activities (RNA) grant number 193133: 'Permafrost Carbon Network: Synthesizing Flux Observations for Benchmarking Model Projections of Permafrost Carbon Exchange (2019–2023)'. Additional funding to E.A.G.S. was provided for data compilation by the NSF Arctic Data Center working group 'Reconciling historical and contemporary trends in terrestrial carbon exchange of the northern permafrost-zone', and the Minderoo Foundation. Many funds supported the data included in this synthesis: A.M.-V., S.M.N., B.M.R., C.M., K.S. and J.D.W. were supported by the Gordon and Betty Moore Foundation (grant number 8414) and through funding catalysed by The Audacious Project (Permafrost Pathways). A.M.-V., B.M.R. and K.S. were also supported by NASA's Arctic–Boreal Vulnerability Experiment and Carbon Cycle Science programmes (NNX17AE13G). F.-J.W.P. was supported by the Research Council of Norway (grant agreement 323945). S.-J.P. was supported by NRF-2021M1A5A1065425 (KOPRI-PN24011). E.L.-B., M.

Mastepanov and T.R.C. were supported by the Greenland Ecosystem Monitoring (GEM) programme. H.D. was supported by the Netherlands Earth System Science Center. M.P., M.B.N. and J.J. acknowledge the Swedish Research Council (VR) for funding to ICOS Sweden and SITES. M.U., H.I., A.K. and H.K. acknowledge the Arctic Challenge for Sustainability II (ArCS II; JPMXD1420318865). N.C. was supported by the NRF-2021M1A5A1065679 and NRF-2021R1I1A1A01053870. I.M. was supported by Research Council of Finland (ICOS-FIRI and N-PERM grant number 341348), ICOS-FI via University of Helsinki funding and the European Union's (EU) Horizon Europe (GreenFeedback number 101056921). B.E. was supported by the Danish National Research Foundation (grant CENPERM DNRF100). M.G. was supported by the European Research Council under the EU Horizon 2020 research and innovation programme (grant agreement number 951288, Q-Arctic) and by the European Climate, Infrastructure and Environment Executive Agency (CINEA) under the Horizon Europe Climate programme (grant agreement number 101056921, GreenFeedback). C.V. was supported by the Academy of Finland project MUFFIN (decision number 332196) and the BMBF project MOMENT (number 03F0931A). E.S.E. and C.W.E. were supported by the National Science Foundation grants DEB LTREB 1354370 and 2011257, DEB-0425328, DEB-0724514, and DEB-0830997, and also by the US Geological Survey Climate R&D Program. E.S.E., C.W.E. and M.S.B.-H. were supported by NSF Arctic Observatory Network grants 1936752, 1503912 and 1107892. C.M. and V.L.S. were supported by the Natural Sciences and Engineering Research Council of Canada (NSERC). L.K. was supported by the Federal Ministry of Education and Research (projects CarboPerm and KoPF, BMBF grant numbers 03G0836A and 03F0764A). L.K. and D.H. were supported by the Cluster of Excellence 'CLICCS—Climate, Climatic Change, and Society' funded by the German Research Foundation (EXC 2037, project number 390683824). A.S.P. and V.I.Z. were supported by the innovative project of national importance (RITM Carbon), registration number 123030300031-6. S.D. and M.S.T. were supported by the US Department of Energy (DOE) Office of Science under contract number DE-AC02-05CH11231 and the DOE Next-Generation Ecosystem Experiments (NGEE Arctic) project. D.Z. was supported by the NSF-AON program (award numbers 1702797 and 1932900).

Author contributions

All authors contributed to data collection and curation. C.R.S. conducted the analyses and wrote the first draft of the article with considerable input from E.A.G.S., A.-M.V., S.M.N., B.M.R., M.G. and M. Mauritz. All authors contributed to subsequent rounds of article revisions.

Competing interests

The authors declare no competing interests.

Additional information

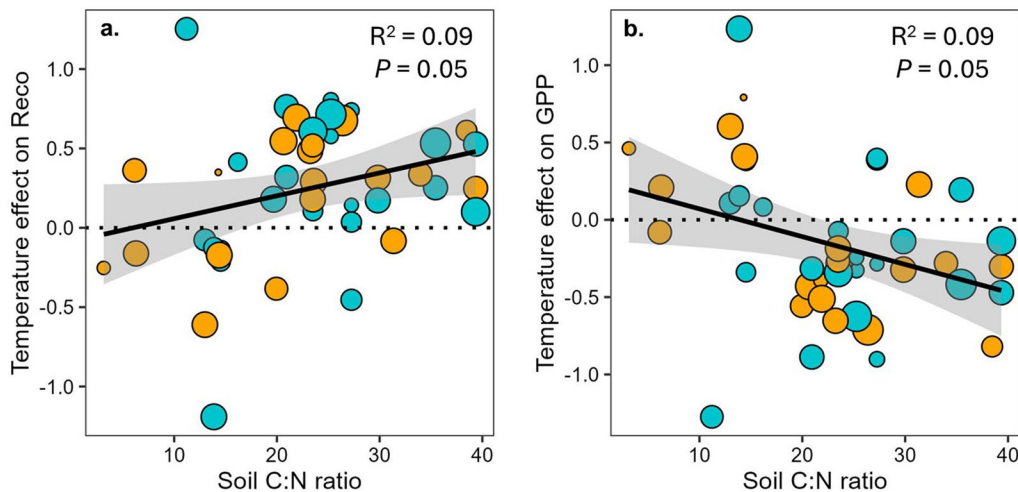
Extended data is available for this paper at <https://doi.org/10.1038/s41558-024-02057-4>.

Supplementary information The online version contains supplementary material available at <https://doi.org/10.1038/s41558-024-02057-4>.

Correspondence and requests for materials should be addressed to Craig R. See.

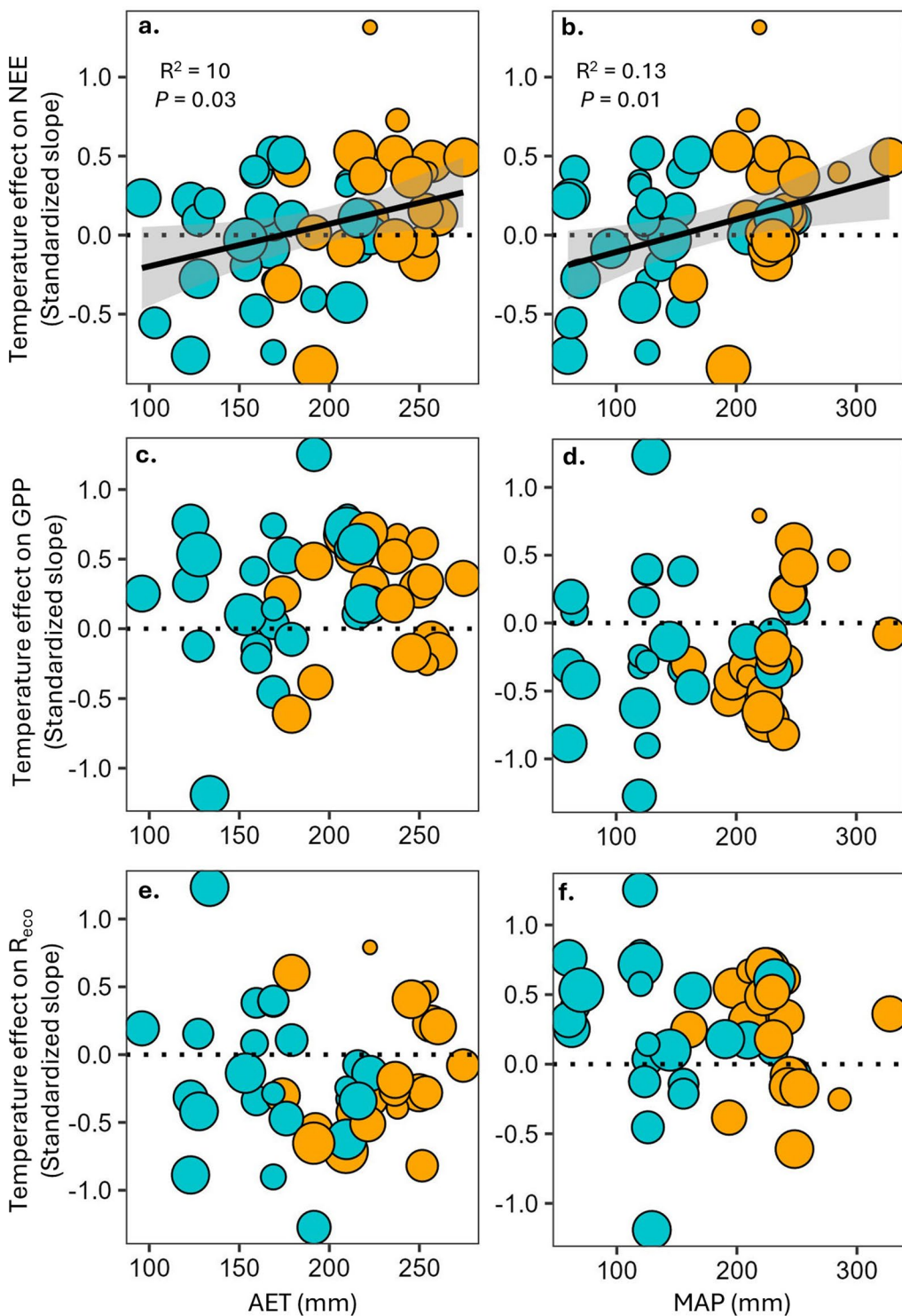
Peer review information *Nature Climate Change* thanks the anonymous reviewer(s) for their contribution to the peer review of this work.

Reprints and permissions information is available at www.nature.com/reprints.



Extended Data Fig. 1 | Soil C:N stoichiometry effects on summer GPP and R_{eco} sensitivity to summer air temperature. Points above the dashed zero line indicate sites where higher than average summer temperatures lead to lower than average GPP (panel a, negative scale, lower plant CO_2 uptake), or higher

than average R_{eco} (panel b, positive scale, greater soil CO_2 losses). Larger points indicate greater confidence in the slope for that site and reflect model weights. Orange points denote nonpermafrost sites, while blue points denote permafrost sites. Error bands represent 95% confidence intervals.



Extended Data Fig. 2 | Sensitivity of summer NEE, GPP, and R_{eco} to summer air temperature, as a function of mean (30-year) summer precipitation (MAP) and mean summer actual evapotranspiration (AET). Points above the dashed zero line indicate sites where higher than average summer temperatures lead to higher than average NEE (that is lower summer CO_2 uptake; panels a, b) or R_{eco}

(panels e, f), and lower than average GPP (panels c, d). Larger points indicate greater confidence in the slope for that site and reflect model weights. Orange points denote nonpermafrost sites, while blue points denote permafrost sites. Error bands represent 95% confidence intervals.